

Mid-Rapidity Neutral Pion Production in Proton-Proton Collisions at $\sqrt{s}=200$ GeV

S.S. Adler,⁵ S. Afanasiev,¹⁷ C. Aidala,⁵ N.N. Ajitanand,⁴³ Y. Akiba,^{20,28} J. Alexander,⁴³ R. Amirikas,¹² L. Aphecetche,⁴⁵ S.H. Aronson,⁵ R. Auerbeck,⁴⁴ T.C. Awes,³⁵ R. Azmoun,⁴⁴ V. Babintsev,¹⁵ A. Baldisseri,¹⁰ K.N. Barish,⁶ P.D. Barnes,³³ B. Bassalleck,³³ S. Bathe,³⁰ S. Batsouli,⁹ V. Baublis,³⁷ A. Bazilevsky,^{39,15} S. Belikov,^{16,15} Y. Berdnikov,⁴⁰ S. Bhagavatula,¹⁶ J.G. Boissevain,²⁷ H. Borel,¹⁰ S. Borenstein,²⁵ M.L. Brooks,²⁷ D.S. Brown,³⁴ N. Bruner,³³ D. Bucher,³⁰ H. Buesching,³⁰ V. Bumazhnov,¹⁵ G. Bunce,^{5,39} J.M. Burward-Hoy,^{26,44} S. Butsyk,⁴⁴ X. Camard,⁴⁵ J.-S. Chai,¹⁸ P. Chand,⁴ W.C. Chang,² S. Chernichenko,¹⁵ C.Y. Chi,⁹ J. Chiba,²⁰ M. Chiu,⁹ I.J. Choi,⁵² J. Choi,¹⁹ R.K. Choudhury,⁴ T. Chujo,⁵ V. Cianciolo,³⁵ Y. Cobigo,¹⁰ B.A. Cole,⁹ P. Constantin,¹⁶ D.G. d'Enterria,⁴⁵ G. David,⁵ H. Delagrange,⁴⁵ A. Denisov,¹⁵ A. Deshpande,³⁹ E.J. Desmond,⁵ O. Dietzsch,⁴¹ O. Drapier,²⁵ A. Drees,⁴⁴ K.A. Drees,⁵ R. du Rietz,²⁹ A. Durum,¹⁵ D. Dutta,⁴ Y.V. Efremenko,³⁵ K. El Chenawi,⁴⁹ A. Enokizono,¹⁴ H. En'yo,^{38,39} S. Esumi,⁴⁸ L. Ewell,⁵ D.E. Fields,^{33,39} F. Fleuret,²⁵ S.L. Fokin,²³ B.D. Fox,³⁹ Z. Fraenkel,⁵¹ J.E. Frantz,⁹ A. Franz,⁵ A.D. Frawley,¹² S.-Y. Fung,⁶ S. Garpman,^{29,*} T.K. Ghosh,⁴⁹ A. Glenn,⁴⁶ G. Gogiberidze,⁴⁶ M. Gonin,²⁵ J. Gosset,¹⁰ Y. Goto,³⁹ R. Granier de Cassagnac,²⁵ N. Grau,¹⁶ S.V. Greene,⁴⁹ M. Grosse Perdekamp,³⁹ W. Guryn,⁵ H.-Å. Gustafsson,²⁹ T. Hachiya,¹⁴ J.S. Haggerty,⁵ H. Hamagaki,⁸ A.G. Hansen,²⁷ E.P. Hartouni,²⁶ M. Harvey,⁵ R. Hayano,⁸ X. He,¹³ M. Heffner,²⁶ T.K. Hemmick,⁴⁴ J.M. Heuser,⁴⁴ M. Hibino,⁵⁰ J.C. Hill,¹⁶ W. Holzmann,⁴³ K. Homma,¹⁴ B. Hong,²² A. Hoover,³⁴ T. Ichihara,^{38,39} V.V. Ikonnikov,²³ K. Imai,^{24,38} L.D. Isenhower,¹ M. Ishihara,³⁸ M. Issah,⁴³ A. Isupov,¹⁷ B.V. Jacak,⁴⁴ W.Y. Jang,²² Y. Jeong,¹⁹ J. Jia,⁴⁴ O. Jinnouchi,³⁸ B.M. Johnson,⁵ S.C. Johnson,²⁶ K.S. Joo,³¹ D. Jouan,³⁶ S. Kametani,^{8,50} N. Kamihara,^{47,38} J.H. Kang,⁵² S.S. Kapoor,⁴ K. Katou,⁵⁰ S. Kelly,⁹ B. Khachaturov,⁵¹ A. Khanzadeev,³⁷ J. Kikuchi,⁵⁰ D.H. Kim,³¹ D.J. Kim,⁵² D.W. Kim,¹⁹ E. Kim,⁴² G.-B. Kim,²⁵ H.J. Kim,⁵² E. Kistenev,⁵ A. Kiyomichi,⁴⁸ K. Kiyoyama,³² C. Klein-Boesing,³⁰ H. Kobayashi,^{38,39} L. Kochenda,³⁷ V. Kochetkov,¹⁵ D. Koehler,³³ T. Kohama,¹⁴ M. Kopytine,⁴⁴ D. Kotchetkov,⁶ A. Kozlov,⁵¹ P.J. Kroon,⁵ C.H. Kuberg,^{1,27} K. Kurita,³⁹ Y. Kuroki,⁴⁸ M.J. Kweon,²² Y. Kwon,⁵² G.S. Kyle,³⁴ R. Lacey,⁴³ V. Ladygin,¹⁷ J.G. Lajoie,¹⁶ A. Lebedev,^{16,23} S. Leckey,⁴⁴ D.M. Lee,²⁷ S. Lee,¹⁹ M.J. Leitch,²⁷ X.H. Li,⁶ H. Lim,⁴² A. Litvinenko,¹⁷ M.X. Liu,²⁷ Y. Liu,³⁶ C.F. Maguire,⁴⁹ Y.I. Makdisi,⁵ A. Malakhov,¹⁷ V.I. Manko,²³ Y. Mao,^{7,38} G. Martinez,⁴⁵ M.D. Marx,⁴⁴ H. Masui,⁴⁸ F. Matathias,⁴⁴ T. Matsumoto,^{8,50} P.L. McGaughey,²⁷ E. Melnikov,¹⁵ F. Messer,⁴⁴ Y. Miake,⁴⁸ J. Milan,⁴³ T.E. Miller,⁴⁹ A. Milov,^{44,51} S. Mioduszewski,⁵ R.E. Mischke,²⁷ G.C. Mishra,¹³ J.T. Mitchell,⁵ A.K. Mohanty,⁴ D.P. Morrison,⁵ J.M. Moss,²⁷ F. Mühlbacher,⁴⁴ D. Mukhopadhyay,⁵¹ M. Muniruzzaman,⁶ J. Murata,^{38,39} S. Nagamiya,²⁰ J.L. Nagle,⁹ T. Nakamura,¹⁴ B.K. Nandi,⁶ M. Nara,⁴⁸ J. Newby,⁴⁶ P. Nilsson,²⁹ A.S. Nyanin,²³ J. Nystrand,²⁹ E. O'Brien,⁵ C.A. Ogilvie,¹⁶ H. Ohnishi,^{5,38} I.D. Ojha,^{49,3} K. Okada,³⁸ M. Ono,⁴⁸ V. Onuchin,¹⁵ A. Oskarsson,²⁹ I. Otterlund,²⁹ K. Oyama,⁸ K. Ozawa,²³ D. Pal,⁵¹ A.P.T. Palounek,²⁷ V.S. Pantuev,⁴⁴ V. Papavassiliou,³⁴ J. Park,⁴² A. Parmar,³³ S.F. Pate,³⁴ T. Peitzmann,³⁰ J.-C. Peng,²⁷ V. Peresedov,¹⁷ C. Pinkenburg,⁵ R.P. Pisani,⁵ F. Plasil,³⁵ M.L. Purschke,⁵ A. Purwar,⁴⁴ J. Rak,¹⁶ I. Ravinovich,⁵¹ K.F. Read,^{35,46} M. Reuter,⁴⁴ K. Reygers,³⁰ V. Riabov,^{37,40} Y. Riabov,³⁷ G. Roche,²⁸ A. Romana,²⁵ M. Rosati,¹⁶ P. Rosnet,²⁸ S.S. Ryu,⁵² M.E. Sadler,¹ N. Saito,^{38,39} T. Sakaguchi,^{8,50} M. Sakai,³² S. Sakai,⁴⁸ V. Samsonov,³⁷ L. Sanfratello,³³ R. Santo,³⁰ H.D. Sato,^{24,38} S. Sato,^{5,48} S. Sawada,²⁰ Y. Schutz,⁴⁵ V. Semenov,¹⁵ R. Seto,⁶ M.R. Shaw,^{1,27} T.K. Shea,⁵ T.-A. Shibata,^{47,38} K. Shigaki,^{14,20} T. Shiina,²⁷ C.L. Silva,⁴¹ D. Silvermyr,^{27,29} K.S. Sim,²² C.P. Singh,³ V. Singh,³ M. Sivertz,⁵ A. Soldatov,¹⁵ R.A. Soltz,²⁶ W.E. Sondheim,²⁷ S.P. Sorensen,⁴⁶ I.V. Sourikova,⁵ F. Staley,¹⁰ P.W. Stankus,³⁵ E. Stenlund,²⁹ M. Stepanov,³⁴ A. Ster,²¹ S.P. Stoll,⁵ T. Sugitate,¹⁴ J.P. Sullivan,²⁷ E.M. Takagui,⁴¹ A. Taketani,^{38,39} M. Tamai,⁵⁰ K.H. Tanaka,²⁰ Y. Tanaka,³² K. Tanida,³⁸ M.J. Tannenbaum,⁵ P. Tarján,¹¹ J.D. Tepe,^{1,27} T.L. Thomas,³³ J. Tojo,^{24,38} H. Torii,^{24,38} R.S. Towell,¹ I. Tserruya,⁵¹ H. Tsuruoka,⁴⁸ S.K. Tuli,³ H. Tydesjö,²⁹ N. Tyurin,¹⁵ H.W. van Hecke,²⁷ J. Velkovska,^{5,44} M. Velkovsky,⁴⁴ L. Villatte,⁴⁶ A.A. Vinogradov,²³ M.A. Volkov,²³ E. Vznuzdaev,³⁷ X.R. Wang,¹³ Y. Watanabe,^{38,39} S.N. White,⁵ F.K. Wohn,¹⁶ C.L. Woody,⁵ W. Xie,⁶ Y. Yang,⁷ A. Yanovich,¹⁵ S. Yokkaichi,^{38,39} G.R. Young,³⁵ I.E. Yushmanov,²³ W.A. Zajc,^{9,†} C. Zhang,⁹ S. Zhou,^{7,51} L. Zolin,¹⁷

(PHENIX Collaboration)

¹Abilene Christian University, Abilene, TX 79699, USA

²Institute of Physics, Academia Sinica, Taipei 11529, Taiwan

³Department of Physics, Banaras Hindu University, Varanasi 221005, India

⁴Bhabha Atomic Research Centre, Bombay 400 085, India

⁵Brookhaven National Laboratory, Upton, NY 11973-5000, USA

⁶University of California - Riverside, Riverside, CA 92521, USA

⁷China Institute of Atomic Energy (CIAE), Beijing, People's Republic of China

⁸Center for Nuclear Study, Graduate School of Science, University of Tokyo, 7-3-1 Hongo, Bunkyo, Tokyo 113-0033, Japan

⁹Columbia University, New York, NY 10027 and Nevis Laboratories, Irvington, NY 10533, USA

- ¹⁰ *Dapnia, CEA Saclay, Bat. 703, F-91191, Gif-sur-Yvette, France*
- ¹¹ *Debrecen University, H-4010 Debrecen, Egyetem tér 1, Hungary*
- ¹² *Florida State University, Tallahassee, FL 32306, USA*
- ¹³ *Georgia State University, Atlanta, GA 30303, USA*
- ¹⁴ *Hiroshima University, Kagamiyama, Higashi-Hiroshima 739-8526, Japan*
- ¹⁵ *Institute for High Energy Physics (IHEP), Protvino, Russia*
- ¹⁶ *Iowa State University, Ames, IA 50011, USA*
- ¹⁷ *Joint Institute for Nuclear Research, 141980 Dubna, Moscow Region, Russia*
- ¹⁸ *KAERI, Cyclotron Application Laboratory, Seoul, South Korea*
- ¹⁹ *Kangnung National University, Kangnung 210-702, South Korea*
- ²⁰ *KEK, High Energy Accelerator Research Organization, Tsukuba-shi, Ibaraki-ken 305-0801, Japan*
- ²¹ *KFKI Research Institute for Particle and Nuclear Physics (RMKI), H-1525 Budapest 114, POBox 49, Hungary*
- ²² *Korea University, Seoul, 136-701, Korea*
- ²³ *Russian Research Center "Kurchatov Institute", Moscow, Russia*
- ²⁴ *Kyoto University, Kyoto 606, Japan*
- ²⁵ *Laboratoire Leprince-Ringuet, Ecole Polytechnique, CNRS-IN2P3, Route de Saclay, F-91128, Palaiseau, France*
- ²⁶ *Lawrence Livermore National Laboratory, Livermore, CA 94550, USA*
- ²⁷ *Los Alamos National Laboratory, Los Alamos, NM 87545, USA*
- ²⁸ *LPC, Université Blaise Pascal, CNRS-IN2P3, Clermont-Fd, 63177 Aubiere Cedex, France*
- ²⁹ *Department of Physics, Lund University, Box 118, SE-221 00 Lund, Sweden*
- ³⁰ *Institut fuer Kernphysik, University of Muenster, D-48149 Muenster, Germany*
- ³¹ *Myongji University, Yongin, Kyonggido 449-728, Korea*
- ³² *Nagasaki Institute of Applied Science, Nagasaki-shi, Nagasaki 851-0193, Japan*
- ³³ *University of New Mexico, Albuquerque, NM, USA*
- ³⁴ *New Mexico State University, Las Cruces, NM 88003, USA*
- ³⁵ *Oak Ridge National Laboratory, Oak Ridge, TN 37831, USA*
- ³⁶ *IPN-Orsay, Universite Paris Sud, CNRS-IN2P3, BP1, F-91406, Orsay, France*
- ³⁷ *PNPI, Petersburg Nuclear Physics Institute, Gatchina, Russia*
- ³⁸ *RIKEN (The Institute of Physical and Chemical Research), Wako, Saitama 351-0198, JAPAN*
- ³⁹ *RIKEN BNL Research Center, Brookhaven National Laboratory, Upton, NY 11973-5000, USA*
- ⁴⁰ *St. Petersburg State Technical University, St. Petersburg, Russia*
- ⁴¹ *Universidade de São Paulo, Instituto de Física, Caixa Postal 66318, São Paulo CEP05315-970, Brazil*
- ⁴² *System Electronics Laboratory, Seoul National University, Seoul, South Korea*
- ⁴³ *Chemistry Department, Stony Brook University, SUNY, Stony Brook, NY 11794-3400, USA*
- ⁴⁴ *Department of Physics and Astronomy, Stony Brook University, SUNY, Stony Brook, NY 11794, USA*
- ⁴⁵ *SUBATECH (Ecole des Mines de Nantes, CNRS-IN2P3, Université de Nantes) BP 20722 - 44307, Nantes, France*
- ⁴⁶ *University of Tennessee, Knoxville, TN 37996, USA*
- ⁴⁷ *Department of Physics, Tokyo Institute of Technology, Tokyo, 152-8551, Japan*
- ⁴⁸ *Institute of Physics, University of Tsukuba, Tsukuba, Ibaraki 305, Japan*
- ⁴⁹ *Vanderbilt University, Nashville, TN 37235, USA*
- ⁵⁰ *Waseda University, Advanced Research Institute for Science and Engineering, 17 Kikui-cho, Shinjuku-ku, Tokyo 162-0044, Japan*
- ⁵¹ *Weizmann Institute, Rehovot 76100, Israel*
- ⁵² *Yonsei University, IPAP, Seoul 120-749, Korea*

(April 28, 2003)

The invariant differential cross section for inclusive neutral pion production in $p+p$ collisions at $\sqrt{s} = 200$ GeV has been measured at mid-rapidity ($|\eta| < 0.35$) over the range $1 < p_T \lesssim 14$ GeV/ c by the PHENIX experiment at RHIC. Predictions of next-to-leading order perturbative QCD calculations are consistent with these measurements. The precision of our result is sufficient to differentiate between prevailing gluon-to-pion fragmentation functions.

PACS numbers: 13.85.Ni, 13.87.Fh, 25.75-q, 25.75.Dw

Particle production at large transverse momenta, p_T , in hadronic reactions has provided an important testing ground for perturbative Quantum Chromodynamics (pQCD) [1]. Next-to-leading order pQCD calculations describe Tevatron ($\sqrt{s}=1.8$ TeV) measurements of inclusive jet production [2] within 10% and direct pho-

ton production [3], in which the elementary quark-gluon scattering produces a photon directly, within 50%. For high- p_T pion production, the recent calculations have not been compared with the UA2 data [4] obtained at $\sqrt{s}=540$ GeV. However, at lower center of mass energies ($\sqrt{s}\lesssim 63$ GeV), they underestimate the data by a factor

of ~ 2.5 [5]. Similar discrepancies have been observed for direct photon measurements from fixed target experiments [6] and have been attributed to effects of soft-gluon radiations beyond NLO [7], to effects of initial intrinsic transverse momentum, k_T [8], or to experimental problems in the difficult direct photon measurements [9,10]. The π^0 calculations, as compared to the jet or direct photon calculations, also require the probability for the scattered quark or gluon to fragment into a pion.

Information on fragmentation to pions [11–15] has principally come from global analyses of inclusive hadron production in e^+e^- annihilation. These analyses constrain the quark-to-pion fragmentation functions well but, via the scale dependence, the gluon-to-pion fragmentation function to a lesser extent. For example, the latter function at a scale of 100 GeV^2 can vary by a factor of 2 to 10 when the fraction of the initial gluon momentum carried by the pion is above 0.5. The more direct measurements of gluon fragmentation functions from b -tagged, three jet event data from LEP [16] have played a limited role in the global analyses because NLO corrections are unavailable for the quantitative treatment, including scale and scheme dependences, of these data. As has been explored for measurements of inclusive hadron production in $p+\bar{p}$ collisions [17], results from inclusive pion production at high p_T can be included in the global analyses and thus may provide meaningful constraints on the gluon-to-pion fragmentation. These results will also provide a reference needed for quantifying the suppression of π^0 production observed in Au-Au collisions at the Relativistic Heavy Ion Collider (RHIC) [18] and, to the extent of agreement with the calculations, the foundations for the planned polarized gluon density measurement with polarized protons in RHIC [19].

In this Letter, we report the first results on inclusive neutral pion production in $p+p$ collisions at a center of mass energy (\sqrt{s}) of 200 GeV as extracted from the data collected during the 2001-2002 run period (Run-2) of RHIC. The bunched proton beams in the collider were vertically polarized with spin orientations alternating in successive bunches. By balancing the integrated luminosity in the different spin states, the effects from polarization were canceled at the 0.1% level.

In Run-2, the PHENIX experiment [20] operated two central arm spectrometers, one muon arm spectrometer, and other detectors for triggering and vertex determination. This work used the beam-beam counters (BBC) [21] for determining the collision vertex and constructing the minimum bias (MB) trigger, and the electromagnetic calorimeters (EMCal) [22] for detecting the neutral pions and deriving high- p_T triggers.

The unbiased differential cross section for π^0 production is calculated from the MB triggered data sample as

$$E \frac{d^3\sigma}{dp^3} = \frac{1}{\hat{\mathcal{L}}} \cdot \frac{1}{2\pi p_T^*} \cdot \frac{C_{\text{reco}} \cdot C_{\text{conv}}}{f_{\pi^0}} \cdot \frac{N_{\pi^0}}{\Delta p_T \Delta y}, \quad (1)$$

where N_{π^0} is the number of π^0 's observed in a Δp_T wide bin at p_T^* defined as the p_T for which the cross section equals its average over the bin; Δy is the rapidity range; C_{reco} is a correction for the acceptance, reconstruction efficiency, and p_T smearing; C_{conv} is a correction for the conversion of decay photons; f_{π^0} is the fraction of the inclusive π^0 yield for which the MB trigger condition was satisfied; and $\hat{\mathcal{L}}$ is the integrated luminosity for the analyzed data sample. The high- p_T triggered sample required an additional correction to account for the efficiency of this trigger for π^0 detection.

The MB trigger imposed the requirement that the collision vertex was within 75 cm of the center of the interaction region. This vertex was reconstructed from the difference in the arrival times of particles at the BBCs which were located along the beam line at ± 1.44 m from the nominal interaction point and subtended the pseudorapidity range $\pm(3.0-3.9)$ with full azimuthal coverage. In the analysis of the data, a more restrictive requirement of ± 30 cm was applied.

The EMCal consisted of two subsystems: a six sector, lead scintillator (PbSc) calorimeter and a two sector, lead glass (PbGl) calorimeter. Located at a radial distance of ~ 5 m from the beam line, each of these sectors covered the pseudorapidity range of $|\eta| < 0.35$ and an azimuthal angle interval of $\Delta\phi \approx 22.5^\circ$. Each of the towers in the calorimeter subtended $\Delta\phi \times \Delta\eta \sim 0.01 \times 0.01$, thus ensuring that the two photons from a decayed π^0 were resolved up to a p_T of at least 20 GeV/ c . The energy calibration was corroborated by the position of the π^0 invariant mass peak, the energy deposit from minimum ionizing charged particles traversing the EMCal (PbSc), and the correlation between the energy deposit in the EMCal and the measured momentum for electrons and positrons identified by the ring-imaging Čerenkov detector. These studies showed that the accuracy of the energy measurement was within 1.5%. At a p_T of ~ 11 GeV/ c , this uncertainty translates into a systematic error on the π^0 yield of $\sim 12\%$. The effective energy resolution for the dataset was deduced from the widths of the π^0 mass peaks, which varied with p_T from 7% to 10% (PbSc) and 12% to 13% (PbGl), and a comparison of the measured energy and momentum for the identified electrons and positrons.

The number of recorded high- p_T π^0 's was enhanced by a high- p_T trigger (denoted as 2×2) in which threshold discrimination was applied independently to sums of the analog signals from non-overlapping, 2×2 groupings (called tiles) of adjacent EMCal towers. During this run, the thresholds corresponded to a deposited energy of 0.75 GeV. The efficiency of this trigger for π^0 detection, $\varepsilon_{\pi^0}^{2 \times 2}(p_T)$, was obtained from the MB data. As shown in Fig. 1a, this efficiency reached a plateau at a p_T of ~ 3 GeV/ c . This dependence was reproduced by Monte Carlo calculations which included the measured tile threshold curves, the EMCal detector response, and

the geometry of the active trigger tiles. The saturation level, 0.78 ± 0.03 for both PbSc and PbGl, was consistent with the geometrical acceptance of the active trigger tiles. For $p_T > 4$ GeV/ c , the geometrical acceptance was used to correct the π° yield in the high- p_T sample.

Since only a fraction of inelastic $p+p$ collisions produce particles which enter both BBCs, the MB trigger condition biased the recorded data sample, so only a fraction, f_{π° , of the inclusive π° yield was detected. This fraction was determined from data collected by an additional, high- p_T trigger which had not been operated in coincidence with the MB trigger. This trigger was formed by threshold discrimination of the sums of the analog signals from overlapping 2×2 groupings of adjacent 2×2 trigger tiles. As shown in Fig. 1b, the fraction of these high- p_T events with π° 's for which the MB condition was also satisfied was 0.75 ± 0.02 , independent of p_T .

In each event, the two photon invariant mass was calculated for each pairing of clusters. Clusters were paired if the energy asymmetry, $|E_1 - E_2|/(E_1 + E_2)$, was less than 0.8 (PbSc) or 0.7 (PbGl). For the PbGl, the pairings were further restricted to those clusters which were identified as electromagetic via the shower profile and time-of-flight. The π° yield was extracted by integrating the invariant mass spectrum over a region around the π° mass. The background contribution in each p_T bin was estimated and then subtracted by fitting the invariant mass distribution outside the peak region (PbSc) or using the mixed event technique (PbGl). For the PbSc and the PbGl, the background to signal ratio varied with increasing p_T from 1 to 0.1 and 1 to 0.03, respectively.

The raw yields were corrected for the p_T smearing arising from the EMCal energy resolution and the steeply falling spectrum; and for the losses due to the disabled towers, the incomplete azimuthal coverage, the energy asymmetry cut, and the photon identification cut (PbGl). The correction for these effects, C_{reco} , was calculated with Monte Carlo simulations which contained the configuration of the active EMCal towers. The energy and position of the decay photons were smeared with the measured test beam resolutions [22] augmented by a constant energy smearing of 5% (12%) for the PbSc (PbGl) to match the response of the EMCal.

The correction for the losses due to conversions of decay photons, C_{conv} , was determined to be 4% (PbSc) and 9% (PbGl) by using a GEANT3 [23] simulation of the PHENIX detector. The same simulation, using $p+p$ events from the PYTHIA generator [24], showed that the contribution of π° 's from secondary interactions was negligible and that the contribution from decays of other hadrons (*e.g.*, K^0 and η mesons) was less than 6%. The π° spectrum was not corrected for these decays.

The integrated luminosity, $\hat{\mathcal{L}}$, was determined from the number of MB events using an absolute calibration of the trigger cross section obtained via the van der Meer scan technique [25]. In a scan, the transverse profile of the

beam overlap is measured by sweeping one beam across the other in steps while monitoring the MB trigger rate. This information, the bunch intensities of the two beams ($\sim 10^{11}$ /bunch), and the revolution frequency (78 kHz) are then used to compute the instantaneous luminosity. The trigger cross section is the ratio of the MB trigger rate when the beams were overlapping maximally to the instantaneous luminosity. Based on three scans, this cross section was 21.8 ± 0.9 (2.8) mb at the 68.5% (95%) confidence level with an absolute error of 0.7 mb. From the linear sum of the absolute error and half of the 95% confidence level, point-to-point systematic error, an error of 9.6% was assigned for the luminosity normalization.

During the run, the maximum and average instantaneous luminosities were 1.5×10^{30} and 0.5×10^{30} $\text{cm}^{-2} \cdot \text{s}^{-1}$, respectively. Contributions from multiple collisions per bunch crossing and beam-gas interactions were negligible. The MB trigger sample of 16 million events corresponded to 0.7 nb^{-1} . As computed from the fraction of recorded MB events which also met the 2×2 high- p_T trigger condition ($\sim 1/47$), the 18 million high- p_T triggered events corresponded to an effective luminosity of 39 nb^{-1} .

The invariant differential cross sections obtained from the MB and high- p_T samples were consistent within the statistical errors over the p_T region of overlap ($p_T \leq 5.5$ GeV/ c). Moreover, the results determined independently from the PbSc and the PbGl data samples were consistent. The main sources of the point-to-point systematic uncertainty in the two measurements are summarized in Table I for a low and a high p_T bin. The total error was computed as the quadrature sum of the statistical and point-to-point systematic errors.

From the MB and the high- p_T trigger samples for p_T below and above 4 GeV/ c , respectively, Table II tabulates the cross section and the errors obtained by averaging the PbSc and PbGl results using the total error for the weighting. Figs. 2a and 2b show this combined result and its fractional statistical and systematic uncertainties ($\Delta\sigma/\sigma$). The data are well parameterized by a power-law form $A \cdot (1 + p_T/p_0)^{-n}$ with parameters of $A=386 \text{ mb} \cdot \text{GeV}^{-2} \cdot c^3$, $p_0=1.219$ GeV/ c , and $n=9.99$.

In Fig. 2, our results are compared with NLO pQCD calculations [26–28]. The basic concept underlying these calculations is the factorization of the cross section into parton distribution functions for the protons, parton-to-pion fragmentation functions, and short-distance partonic hard-scattering cross sections which can be evaluated using perturbative QCD. Because of this factorization, the calculations depend on unphysical, factorization and renormalization scales which are of the order of the hard scale p_T . This dependence is reduced as higher order terms are included in the perturbation expansion. For a calculation truncated at a given order, this dependence serves as a gauge for the uncertainty in its results.

The calculations in Fig. 2 have been performed with equal renormalization and factorization scales of $p_T/2$,

p_T , and $2p_T$ by using the CTEQ6M [29] set of parton distribution functions and two sets of fragmentation functions. In general, these calculations are consistent with the data, even at low p_T (<2 GeV/ c) where the theory might be expected to be less applicable. On closer inspection, as shown Fig. 2c and 2d, the calculation with the “Kniehl-Kramer-Pötter” (KKP) set of fragmentation functions [12] agrees with our data better than the calculation with the “Kretzer” set [13] does. These two sets differ mainly in that the gluon-to-pion fragmentation function, D_g^π , is greater in the KKP set. This difference is exhibited primarily at low p_T because of the dominance of gluon-gluon and gluon-quark interactions for p_T below ~ 10 GeV/ c [26]. Our measurement thus may impose a meaningful constraint on D_g^π .

In summary, the invariant differential cross section for inclusive neutral pion production in $p+p$ collisions at $\sqrt{s}=200$ GeV was measured at mid-rapidity ($|\eta| < 0.35$) as a function of p_T up to ~ 14 GeV/ c . These results were compared with two NLO pQCD calculations which differed in the choice of fragmentation functions. Over the full range of p_T , the calculations were consistent with the result within the uncertainty of the calculations as judged from the scale dependence, although the results favored a larger gluon-to-pion fragmentation function.

We thank the staff of the Collider-Accelerator and Physics Departments at BNL for their vital contributions. We thank Werner Vogelsang and Stefan Kretzer for their interest and input. We acknowledge support from the Department of Energy and NSF (U.S.A.), MEXT and JSPS (Japan), CNPq and FAPESP (Brazil), NSFC (China), CNRS-IN2P3 and CEA (France), BMBF, DAAD, and AvH (Germany), OTKA (Hungary), DAE and DST (India), ISF (Israel), KRF and CHEP (Korea), RAS, RMAE, and RMS (Russia), VR and KAW (Sweden), U.S. CRDF for the FSU, US-Hungarian NSF-OTKA-MTA, and US-Israel BSF.

* Deceased

† Spokesperson: zajc@nevis.columbia.edu

[1] J. F. Owens, Rev. Mod. Phys. **59** 465 (1987).

[2] D. Stump *et al.*,

[\protect\vrule width0pt\protect\href{http://arXiv.org/abs/hep-ph/0303013}](http://arXiv.org/abs/hep-ph/0303013){hep-ph/0303013}.

[3] D. Acosta *et al.* [CDF Collaboration], Phys. Rev. **D65**, 112003 (2002); V.M. Abazov *et al.* [D0 Collaboration], Phys. Rev. Lett. **87**, 251805 (2001).

[4] M. Banner *et al.* [UA2 Collaboration], Phys. Lett. **B115** 59 (1982).

[5] P. Aurenche *et al.*, Eur. Phys. J. **C13**, 347 (2000).

[6] W. Vogelsang and M.R. Whalley, J. Phys. G: Nucl. Part. Phys. **23**, A1 (1997).

[7] E. Laenen *et al.*, Phys. Rev. **D63**, 114018 (2001).

[8] L. Apanasevich *et al.*,

[\protect\vrule width0pt\protect\href{http://arXiv.org/abs/h](http://arXiv.org/abs/h)

[9] P. Aurenche *et al.*, Eur. Phys. J. **C9**, 107 (1999).

[10] L. Apanasevich *et al.*, Phys. Rev. **D63**, 014009 (2001).

[11] J. Binnewies, B.A. Kniehl, and G. Kramer, Phys. Rev. **D52**, 4947 (1995).

[12] B.A. Kniehl *et al.*, Nucl. Phys. **B597**, 337 (2001).

[13] S. Kretzer, Phys. Rev. **D62**, 054001 (2000).

[14] S. Kretzer *et al.*, Eur. Phys. J. **C22**, 269 (2001).

[15] O. Biebel *et al.*,

[\protect\vrule width0pt\protect\href{http://arXiv.org/abs/h](http://arXiv.org/abs/h)

[16] P. Abreu *et al.* [DELPHI Collaboration], Eur. Phys. J. **C17**, 207 (2000); G. Abbiendi *et al.* [OPAL Collaboration], Eur. Phys. J. **C11**, 217 (1999); R. Barate *et al.* [ALEPH Collaboration], Eur. Phys. J. **C17**, 1 (2000).

[17] L. Bourhis *et al.*, Eur. Phys. J. **C19** 89 (2001).

[18] S.S. Adler *et al.* [PHENIX Collaboration], submitted to Phys. Rev. Lett.

[19] G. Bunce *et al.*, Ann. Rev. Nucl. Part. Sci. **50**, 525 (2000).

[20] PHENIX NIM paper Nucl. Instrum. Methods **A**.

[21] M. Allen *et al.*, to appear in Nucl. Instrum. Methods **A**.

[22] L. Aphecetche *et al.*, Nucl. Instrum. Methods **A499**, 521 (2003).

[23] GEANT 3.21, CERN program library.

[24] T. Sjöstrand, Comp. Phys. Commun. **82**, 74 (1994).

[25] K. A. Drees and Z. Xu, “Proceedings of the PAC2001 Conference,” 3120 (2001).

[26] F. Aversa *et al.*, Nucl. Phys. **B327**, 105 (1989); *n.b.*,

these authors wrote the computer code used for our calculations.

[27] B. Jäger *et al.*, Phys. Rev. **D67**, 054005 (2003).

[28] D. de Florian, Phys. Rev. **D67**, 054004 (2003).

[29] J. Pumplin *et al.* [CTEQ Collaboration], J. High Energy Phys. **0207**, 012 (2002).

TABLE I. Summary of the sources of systematic errors on the π^0 yields and the total systematic error for p_T of 1.2 and 10.9 GeV/ c . The normalization error of 9.6% is not listed.

p_T (in GeV/ c)	% Error (PbSc)		% Error (PbG1)	
	1.2	10.9	1.2	10.9
Energy Scale	3	11	6	12
Yield Extraction	7	4	5	5
Yield Correction	3	6	6	11
Acceptance Stability	4.5	4.5	3	2
Total	9	14	10	17

TABLE II. The p_T^* (see text for definition), the invariant differential cross section for inclusive neutral pion production in $p+p$ collisions at $\sqrt{s}=200$ GeV, the statistical uncertainty, and the systematic uncertainty for each p_T bin. The absolute normalization error of 9.6% is not included.

p_T bin (GeV/c)	p_T^* (GeV/c)	inv. cross section (mb·GeV ⁻² ·c ³)	stat. error (%)	syst. error (%)
1.0-1.5	1.22	$3.73 \cdot 10^{-1}$	1.6	7.3
1.5-2.0	1.72	$6.05 \cdot 10^{-2}$	1.8	7.1
2.0-2.5	2.22	$1.22 \cdot 10^{-2}$	2.5	7.1
2.5-3.0	2.73	$3.31 \cdot 10^{-3}$	3.6	7.2
3.0-3.5	3.23	$9.98 \cdot 10^{-4}$	5.7	7.3
3.5-4.0	3.73	$3.39 \cdot 10^{-4}$	7.3	7.7
4.0-4.5	4.23	$1.19 \cdot 10^{-4}$	2.4	8.3
4.5-5.0	4.73	$4.73 \cdot 10^{-5}$	4.2	8.5
5.0-5.5	5.23	$2.21 \cdot 10^{-5}$	5.0	8.7
5.5-6.0	5.74	$1.11 \cdot 10^{-5}$	4.5	9.2
6.0-6.5	6.24	$5.00 \cdot 10^{-6}$	6.3	9.5
6.5-7.0	6.74	$3.00 \cdot 10^{-6}$	7.7	9.8
7.0-8.0	7.45	$1.08 \cdot 10^{-6}$	8.8	10.1
8.0-9.0	8.46	$4.85 \cdot 10^{-7}$	12.0	10.8
9.0-10.0	9.46	$1.64 \cdot 10^{-7}$	19.3	11.0
10.0-12.0	10.86	$5.07 \cdot 10^{-8}$	22.3	11.7
12.0-15.0	13.25	$9.76 \cdot 10^{-9}$	41.3	15.6

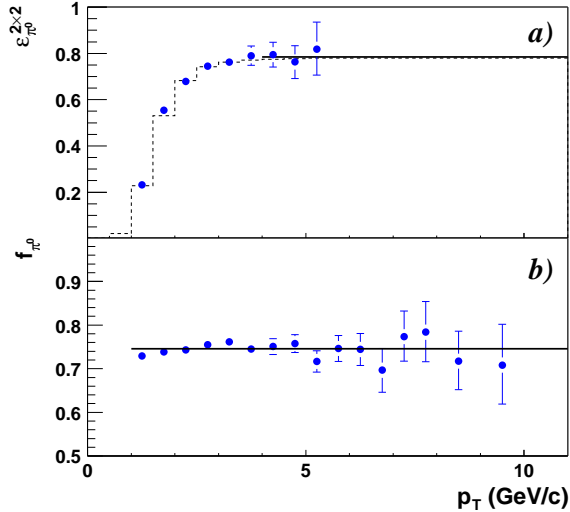


FIG. 1. a) The efficiency of the 2×2 high- p_T trigger for π^0 's as a function of the p_T of the π^0 . The dashed and solid lines show the results of a Monte Carlo simulation based on the 2×2 trigger tile efficiencies and the limit derived from the fraction of active trigger tiles, respectively. b) The fraction of the inclusive π^0 yield which satisfied the MB trigger condition. The solid line shows a fit of these data to a constant.

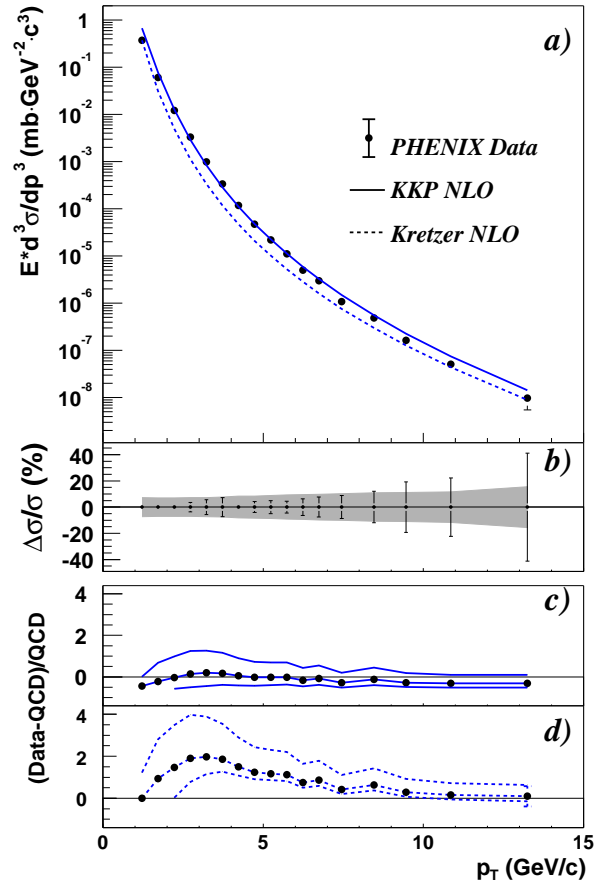


FIG. 2. a) The invariant differential cross section for inclusive π^0 production (points) and the results from NLO pQCD calculations with equal renormalization and factorization scales of p_T using the “Kniehl-Kramer-Pötter” (solid line) and “Kretzer” (dashed line) sets of fragmentation functions. b) The relative statistical (points) and point-to-point systematic (band) errors. c,d) The relative difference between the data and the theory using KKP (c) and Kretzer (d) fragmentation functions with scales of $p_T/2$ (lower curve), p_T , and $2p_T$ (upper curve). In all figures, the normalization error of 9.6% is not shown.